

DualFormer: Local-Global Stratified Transformer for Efficient Video Recognition

Yuxuan Liang^{1,2*} Pan Zhou¹ Roger Zimmermann² Shuicheng Yan¹

¹Sea AI Lab ²National University of Singapore

{liangyx, zhoupan, ysc}@sea.com {rogerz}@comp.nus.edu.sg

Abstract

While transformers have shown great potential on video recognition tasks with their strong capability of capturing long-range dependencies, they often suffer high computational costs induced by self-attention operation on the huge number of 3D tokens in a video. In this paper, we propose a new transformer architecture, termed DualFormer, which can effectively and efficiently perform space-time attention for video recognition. Specifically, our DualFormer stratifies the full space-time attention into dual cascaded levels, i.e., to first learn fine-grained local space-time interactions among nearby 3D tokens, followed by the capture of coarse-grained global dependencies between the query token and the coarse-grained global pyramid contexts. Different from existing methods that apply space-time factorization or restrict attention computations within local windows for improving efficiency, our local-global stratified strategy can well capture both short- and long-range spatiotemporal dependencies, and meanwhile greatly reduces the number of keys and values in attention computation to boost efficiency. Experimental results show the superiority of DualFormer on five video benchmarks against existing methods. In particular, DualFormer sets new state-of-the-art 82.9%/85.2% top-1 accuracy on Kinetics-400/600 with $\sim 1000G$ inference FLOPs which is at least $3.2\times$ fewer than existing methods with similar performances.

1. Introduction

Video recognition is a fundamental task in computer vision, such as action recognition [5] and event detection [21]. Like in image-based tasks [20, 30, 45], Convolutional Neural Networks (CNNs) are often taken as backbone for video recognition models [6, 14, 15, 34, 49, 51]. Though successful, it is challenging for convolutional architectures to capture long-range spatiotemporal dependencies across video frames due to their limited receptive field.

*This work was done when the first author was an intern at Sea AI Lab.

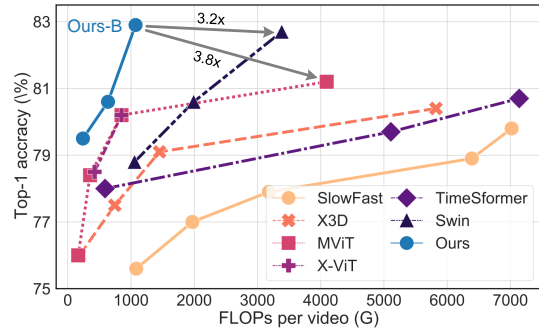


Figure 1. Accuracy vs. FLOPs on Kinetics-400.

Recently, Transformers [52] have presented an alternative visual modeling paradigm beyond CNNs, demonstrating great potential in many image processing tasks [36, 43, 53, 55, 57, 64]. A pioneering work is the Vision Transformer (ViT) [12], which replaces the inherent inductive bias of locality in convolutions by global relation modeling with multi-head self-attention (MSA) [52]. Soon the vision community extended the application of MSA from static images to videos considering its remarkable power for capturing long-range spatiotemporal dependencies [1, 3, 13, 40]. To be more specific, a video is first partitioned into non-overlapping 3D patches, similar as in NLP tasks [52], which then serve as input tokens for transformers to jointly learn short and long-range relations within a video.

One of the major challenges when applying transformers to video data is their *efficiency*. Due to the MSA operation, the computational costs of video transformers grows quadratically with the increasing number of tokens, and may even become totally unaffordable for some high spatial resolution or long videos. To alleviate this issue, some studies [1, 3] factorize the full space-time self-attention along temporal and spatial dimensions, achieving a better balance between speed and accuracy in video recognition. Another work [38] proposes a Video Swin Transformer that applies the inductive bias of locality at every layer of ViTs by restricting the self-attention computation to non-overlapping local windows, inspired by the observation that near objects are usually more related than distant ones [47]. Though

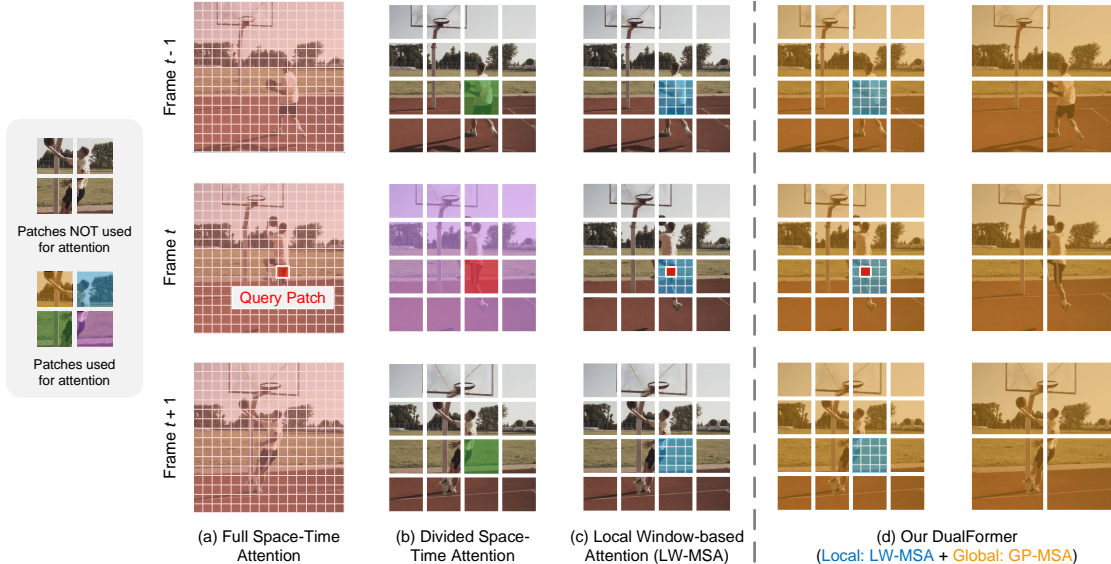


Figure 2. Visualization of four space-time MSA schemes. For better illustration, we use 2D patch partitions here. We denote in red the query patch and in non-red colors its attention targets for each scheme (see the legend on the left). **Multiple highlighted colors within a scheme indicate the MSA separately applied along different dimensions.** (a) Full space-time attention [3], which has quadratic complexity w.r.t. the number of patches. (b) Divided space-time attention [3], where MSA is separately applied in temporal and spatial domains, with a larger patch size used for cost reduction. (c) Local window-based attention [38], which improves efficiency by restricting MSA computation within local windows. However, it lacks the interactions between distant patches due to small receptive fields. (d) Our dual-level MSA scheme that stratifies the modeling of local and global relations. Given a query patch, we first use LW-MSA to compute attention weights within the local window. Then, the query patch attends to the multi-scale global priors (two scales here) via GP-MSA.

effective, both the space-time factorization and the local window-based attention scheme contradict the aim of applying full space-time attention, i.e., to *jointly* capture local and global spatiotemporal dependencies within one layer.

In this paper, we present a new transformer architecture entitled **DualFormer** for efficient video recognition, which *stratifies* the full space-time attention into dual cascaded levels – 1) *Local Window-based Attention* (LW-MSA) for extracting short-range interactions among nearby tokens; and 2) *Global Pyramid-based Attention* (GP-MSA) for capturing long-range dependencies between the query token and the coarse-grained global pyramid contexts. In this manner, our method can significantly reduce the number of keys and values in attention computation, thereby achieving a better speed-accuracy trade-off than existing video transformers [1, 3, 38], as shown in Figure 1.

Figure 2 illustrates how a query patch (in red) attends to its surroundings in the proposed DualFormer block versus existing methods. Following the intuition that tokens closer to each other are more likely to be correlated [9, 30, 36, 60], we first perform LW-MSA at a fine-grained level to allow each patch to interact with its neighbors within a local window. This strategy has also been verified to be efficient and memory-friendly by recent studies [7, 9, 36, 38, 60]. Next, at the global level, a query patch attends to the full region of interest at a coarse granularity via GP-MSA. Specifically, we first extract global contextual priors with differ-

ent pyramid scales for multi-scale scene interpretation (see the two scales in Figure 2(d)). These global priors then pass global contextual information to the query tokens via MSA. Note that the number of global priors is much fewer than the original token number, GP-MSA thereby induces far fewer computation costs in capturing global information than the full space-time attention. In contrast to the space-time factorization [1, 3] and the locality-based scheme [38], this dual-level attention design not only enables our model to have the global receptive field at each block, but is also efficient in MSA computations.

We conduct extensive experiments on five popular video benchmarks to validate the superiority of our DualFormer in terms of accuracy and FLOPs. In particular, our DualFormer achieves 82.9%/85.2% top-1 accuracy on Kinetics-400/600 [28] with only ~ 1000 GFLOPs which is $3.2\times$ and $16.2\times$ fewer than the previous state-of-the-art methods Swin [36] and ViViT [1], respectively. More details on Kinetics-400 can be seen in Figure 1. We also show how we can effectively leverage our model to yield state-of-the-art performance on three smaller datasets via transfer learning.

2. Related Work

2.1. CNN-based Video Recognition

CNN-based video recognition models can be categorized into two groups: 2D CNNs and 3D CNNs [33]. For the first

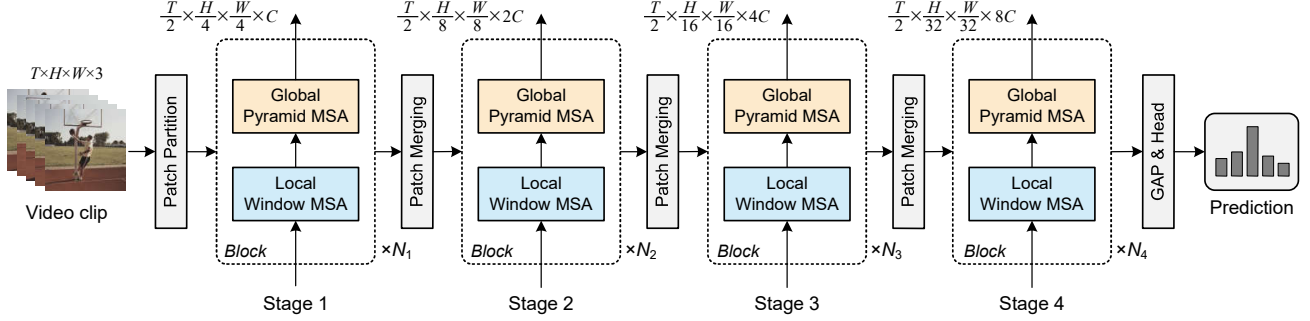


Figure 3. Overall architecture of our approach. GAP: global average pooling.

group of methods [27, 54], each video frame is processed separately by 2D convolutions and then aggregated along the time axis at the top of the network. However, some studies point out that 2D convolutions cannot well capture the information along the temporal dimension [24, 34, 37, 39]. The second group of methods learn spatiotemporal video representation via 3D convolutions by aggregating space-time features and are difficult to optimize [17, 18, 23, 49, 59]. Thus, the current trend for 3D CNN-based video recognition is to boost efficiency. For example, I3D [6] expands pretrained 2D CNNs [20, 30, 45] into 3D CNNs; some recent works [14, 15, 42, 50, 51, 58] factorize 3D convolutions into spatial and temporal filters, demonstrating even higher accuracy than vanilla 3D CNNs. Unfortunately, most of the 2D and 3D CNNs cannot capture long-range spatiotemporal dependencies due to their limited receptive fields, which leads to sub-optimal recognition performance.

2.2. Transformer-based Video Recognition

Recently, transformers are applied to model spatiotemporal dependencies for video recognition [1, 3, 4, 13, 38, 40, 41, 62, 63] by virtue of their great power in capturing long-range dependencies [9, 12, 36, 48]. With pretraining on a large-scale image dataset, video transformers achieve the best reported accuracy on video benchmarks [1, 3, 38], such as Kinetics-400/600 [28]. However, the potential of video transformers is significantly limited by the considerable computational complexity of performing full space-time attention. Various approaches have been proposed to reduce such computation costs [1, 3, 4, 38, 63]. For instance, TimeSformer [3] factorizes the full space-time attention into spatial and temporal dimensions. Likewise, ViViT [1] examines three variants of space-time factorization for computation reduction. X-ViT [4] approximates the space-time attention by restricting the temporal attention to a local temporal window and using a mixing strategy. Video Swin Transformer [38] creatively introduces an inductive bias of locality to transformers for video understanding. However, these attempts focus on either the space-time factorization or restricting attention computation locally, crippling the capability of MSA in capturing long-range dependencies. To

address this issue, we present a new transformer called DualFormer to improve the efficiency of video transformers. Different from existing arts, it alternatively captures fine-grained local interactions and coarse-grained global information within a DualFormer block, resulting in a huge reduction of keys and values in attention computations.

3. Methodology

We start by summarizing the overall architecture of DualFormer in Sec. 3.1, and then elaborate on its basic block in Sec. 3.2 by well introducing the two types of attention, including Local Window-based MSA (LW-MSA) and Global Pyramid-based MSA (GP-MSA). Afterwards, we describe the Position Encoding Generator (PEG) in Sec. 3.3 and discuss the differences between our DualFormer and its related works in Sec. 3.4. Finally, we give the network configuration for constructing our DualFormer in Sec. 3.5.

3.1. Overall Architecture

Figure 3 shows the overall architecture of the proposed DualFormer. It takes a video clip $\mathcal{X} \in \mathbb{R}^{T \times H \times W \times 3}$ as input, where T stands for the number of frames and each frame consists of $H \times W \times 3$ pixels. To accommodate high-resolution video-based tasks, our model leverages a hierarchical design [13, 36, 38, 60] to produce decreasing-resolution feature maps from early to late stages. First, we partition a video clip into non-overlapping 3D patches of size $2 \times 4 \times 4 \times 3$ and employ a linear layer for projection, resulting in $\frac{T}{2} \times \frac{H}{4} \times \frac{W}{4}$ visual tokens with C feature channels. These tokens then go through the four stages of DualFormer, as shown in Figure 3, for learning visual representations. At each stage $i \in \{1, 2, 3, 4\}$, we sequentially stack N_i DualFormer blocks for spatiotemporal learning, where N_i controls the capacity of each model stage. Each DualFormer block consists of dual cascaded levels of self-attention mechanisms: LW-MSA for learning short-range interactions within local windows, and GP-MSA for capturing long-range context information within the whole video. Besides, a convolution-based Position Encoding Generator (PEG) is integrated at each stage to em-

power position-aware MSA. After each stage, DualFormer follows the prior art [38] to utilize a patch merging layer to downsample the spatial size of the feature map by $2\times$, while the feature channel dimension is increased by $2\times$. Once the output of the last stage is obtained, DualFormer performs the video recognition by applying a global average pooling (GAP) layer followed by a linear classifier.

3.2. DualFormer Block

Given an input feature map of $T' \times H' \times W'$ resolution with D dimensions, the complexity of full space-time attention is $\mathcal{O}((T'H'W')^2D)$, making it impractical to accommodate high-resolution videos. In a DualFormer block, we stratify the full space-time attention into dual cascaded levels (LW-MSA and GP-MSA) to alleviate this issue.

3.2.1 Local Window-based MSA

Considering nearby tokens often have stronger correlations than faraway tokens, we perform LW-MSA to compute the self-attention within non-overlapping 3D windows to capture local interactions among tokens. Given a feature map with $T' \times H' \times W'$ patches, we first evenly split it into small windows, each containing $t \times h \times w$ patches (like Figure 2d), leading to $\frac{T'}{t} \times \frac{H'}{h} \times \frac{W'}{w}$ windows. Assume the flattened tokens within a window (i, j, k) are denoted as $\mathbf{X}_{i,j,k} \in \mathbb{R}^{thw \times D}$. LW-MSA is formulated as

$$\begin{aligned} \mathbf{X}'_{ijk} &= \text{MSA}(\text{LN}(\mathbf{X}_{ijk})) + \mathbf{X}_{ijk}, \\ \mathbf{Y}'_{ijk} &= \text{MLP}(\text{LN}(\mathbf{X}'_{ijk})) + \mathbf{X}'_{ijk}, \end{aligned} \quad (1)$$

where LN is layer normalization [2] for achieving smoother gradients, and MLP indicates a multi-layer perceptron for non-linear transformation. As the computational complexity¹ of MSA within a local window is $\mathcal{O}((thw)^2D)$, the total cost of LW-MSA is computed as

$$\mathcal{O}(\text{LW-MSA}) = (thw)^2D \times \frac{T'H'W'}{thw} = thwMD \quad (2)$$

where $M = T'H'W'$ is the token number. Compared to the full space-time attention with $\mathcal{O}(M^2D)$, Eq. (2) is much more efficient ($\frac{M}{thw}$ times less) when $t \ll T$, $h \ll H$ and $w \ll W$ and grows linearly with M if t, h, w are fixed. We will show the effect of t, h, w in Sec. 4.4.

3.2.2 Global Pyramid-based MSA

While being efficient in computation, LW-MSA cripples the ability of MSA to capture global information. For example, a query patch cannot attend to a patch outside the local window. To tackle this problem, a shifted window strategy is proposed to enable a patch to communicate with the patches inside adjacent windows in [38]. Nevertheless, it is

¹For simplicity, we omit the complexity of MLP in this paper.

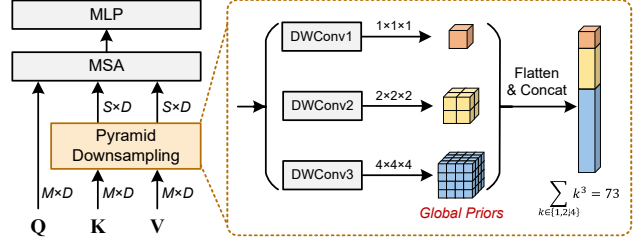


Figure 4. The pipeline of GP-MSA. DWConv denotes depth-wise convolution for generating global priors with multiple scales. For simplicity, we use a three-level pyramid ($1 \times 1 \times 1$, $2 \times 2 \times 2$, and $4 \times 4 \times 4$) for illustration. With pyramid downsampling, the computational cost and memory usage of GP-MSA are much lower than those of standard MSA due to reduction of the key/value number, which is more friendly to high-resolution or long videos.

still difficult for patches to interact with distant windows. In this work, we devise GP-MSA as a complement for learning long-range dependencies within the whole video.

Model Design. As a variant of vanilla MSA, our GP-MSA receives a query \mathbf{Q} , a key \mathbf{K} , and a value \mathbf{V} as input to capture the global information. For simplicity, we assume \mathbf{Q} , \mathbf{K} and \mathbf{V} are all in shape $M \times D$, where M is the number of tokens. Different from the vanilla MSA, our GP-MSA applies a simple yet effective method named *pyramid downsampling* to reduce the spatiotemporal scale of \mathbf{K} and \mathbf{V} before performing MSA, so as to lessen the computational overheads and memory usage. Such efficient design is inspired by the spatial pyramid pooling [19] which employs adaptive average pooling to produce consistent length representations for any resolution images. Compared with spatial pyramid pooling, our pyramid downsampling is aimed at generating multi-scale global priors via convolutions.

As depicted in Figure 4, our pyramid downsampling applies three levels of depth-wise convolutions to generate a set of global priors, where each prior is a spatiotemporal abstract of the original feature map under different pyramid scales. This operation allows the model to separate the feature map into non-overlapping regions and build pooled representations for various locations. For example, the $1 \times 1 \times 1$ prior (the orange cube) denotes the coarsest scale with only a single value at each channel, which is similar to global average pooling [35] that covers the whole video, while the $2 \times 2 \times 2$ prior (the yellow cube) indicates a summary of finer granularity. Then, we flatten and concatenate these priors to be the new key-value with size $S \times D$, where S stands for the number of space-time locations, e.g., $S = \sum_{k \in \{1,2,4\}} k^3 = 73$ in Figure 4. After pyramid downsampling, standard MSA is performed to allow these global priors to pass global contextual information to each query patch.

Complexity Analysis. Without loss of generality, suppose we have N_g pyramid scales and denote the size of global prior at the i -th scale as (k_1^i, k_2^i, k_3^i) , where $k_1^i < T'$, $k_2^i <$

H' and $k_3^i < W'$. The complexity of GP-MSA is

$$\begin{aligned} \mathcal{O}(\text{GP-MSA}) &= MD \underbrace{\sum_{i=1}^{N_g} k_1^i k_2^i k_3^i}_{\text{MSA}} + \underbrace{\sum_{i=1}^{N_g} \left(\frac{T' H' W'}{k_1^i k_2^i k_3^i} k_1^i k_2^i k_3^i D \right)}_{\text{DWConv}} \\ &= \left(\sum_{i=1}^{N_g} k_1^i k_2^i k_3^i + N_g \right) MD = (S + N_g) MD, \end{aligned}$$

where $S = \sum_{i=1}^{N_g} k_1^i k_2^i k_3^i$ is the number of global priors, i.e., new keys or values after reduction. To further improve efficiency, we draw inspiration from R(2+1)D [51] to factorize the depth-wise convolution at each scale along temporal and spatial dimensions, resulting in even less complexity:

$$\begin{aligned} \mathcal{O}(\text{GP-MSA}) &= \left(S + \sum_{i=1}^{N_g} \left(\frac{k_1^i}{T'} + \frac{k_2^i k_3^i}{H' W'} \right) \right) MD \\ &\approx SMD \ll \underbrace{(S + N_g) MD}_{\text{Previous}} \ll \underbrace{M^2 D}_{\text{MSA}}. \end{aligned} \quad (3)$$

Since S is generally much fewer than the number of tokens (M) in the original feature map, our GP-MSA significantly reduces the computational complexity and memory usage in learning global representations. For instance, at the first stage of DualFormer where S is 456 while M is 50176, the complexity has been reduced by ~ 110 times. In a nutshell, the overall complexity of MSA in a DualFormer block is the summation of LW-MSA in Eq. (2) and GP-LSA in Eq. (3).

3.3. Position Encoding Generator

As the self-attention operation is permutation-invariant, various position encoding methods are proposed to provide position information in video transformers. Absolute position embedding [52] is the most popular approach in the mainstream of video transformers [1, 3, 4, 13], which is added to the tokens to retain positional information and is updated during the training phase. On the contrary, Video Swin Transformer [38] incorporates the position knowledge by including a relative position bias to each head in self-attention computation. However, either absolute or relative position encoding cannot well collocate with the data augmentation [9, 10], such as rotation and shifting. To enable translation-invariance, we propose to employ a simple yet effective convolution-based PEG at the first block of each stage (inserted between the two types of MSA) as follows:

$$\text{PEG}(\mathbf{X}) = \text{DWConv}(\mathbf{X}) + \mathbf{X}, \quad (4)$$

where \mathbf{X} is the input of the current stage. $\text{DWConv}(\cdot)$ represents 3D depth-wise convolution [8]. By using convolutions, the position embedding is no longer input-agnostic and dynamically generated based on the local neighbors of each token. Moreover, such PEG can be easily plugged into existing video transformers with negligible costs.

3.4. Discussion

Comparison with Space-Time Factorization. In contrast to TimeSformer [3] and ViViT [1] that separately adopt MSA in temporal and spatial domains, our DualFormer factorizes the full space-time attention along another two dimensions — local and global dependencies. Hence, our method can attend to any region of interest within the 3D feature map via GP-MSA, while TimeSformer and ViViT can only learn separate spatial or temporal information at each layer due to the space-time factorization.

Comparison with Video Swin. Swin [38] makes the first attempt to leverage window-based MSA for video recognition, achieving state-of-the-art performance on three benchmarks. To enable cross-window communication, it applies a shifting strategy to increase the receptive field. However, it still lacks the connections between distant patches, contradicting the intention of MSA. In contrast, our method follows a local-to-global paradigm which has achieved much success in vision tasks [7, 9, 56]. Our method not only preserves global receptive field at each block, but is also efficient in computation, as shown in the above analysis.

Comparison with Image-based ViTs. Our DualFormer can be also linked to several image-based transformers with a local-global stratified design, including RegionViT [7] and Twins-SVT [9]. The major difference between our approach and RegionViT lie in two aspects. First, the regional tokens in RegionViT are produced at the beginning of the neural networks and updated at every block, while DualFormer generates the global contextual priors for each block separately. Second, RegionViT utilizes an absolute position embedding to allow position-aware MSA. In contrast, we propose a convolution-based PEG which dynamically generates the position embedding based on the local neighbors of each token. Compared to Twins-SVT, the major difference is the construction of global contexts. Since the objects across different frames in a video may vary in sizes, our DualFormer extracts multi-scale global contextual information via a pyramid downsampling module, while Twins-SVT only captures global information at a specific scale.

3.5. Model Configuration

Following Video Swin Transformer [38], we consider three network configurations (i.e., base, small and tiny) for our DualFormer. For all versions, the window size in LW-MSA is fixed (8, 7, 7), and the MLP expansion factor is 4. In GP-MSA, we utilize two pyramid scales (8, 7, 7) and (4, 4, 4) at the first two stages for learning global contextual information. At the last two stages, as the resolution of the feature map has been reduced significantly, we propose to extract a single scale of global contextual priors to reduce computational costs. More details about the model configuration can be found in Appendix A.4.

Method	Pretrain	Input	Views	Overall FLOPs	Param	Kinetics-400		Kinetics-600	
						Top-1	Top-5	Top-1	Top-5
R(2+1)D [51]	-	32×2	10×1	750	61.8	72.0	90.0	-	-
I3D [6]	ImageNet-1K	32×2	-	108	25.0	72.1	90.3	-	-
SlowFast+NL [15]	-	-	10×3	7020	59.9	79.8	93.9	81.8	95.1
X3D-XL [14]	-	16×5	10×3	1452	11.0	79.1	93.9	81.9	95.5
X3D-XXL [14]	-	16×5	10×3	5823	20.3	80.4	94.6	-	-
ip-CSN-152 [50]	IG-65M	8	10×3	3270	32.8	82.5	95.3	-	-
ViT-B-VTN [40]	ImageNet-21K	250×1	1×1	4218	11.0	78.6	93.7	-	-
TimeSformer-L [3]	ImageNet-21K	96×4	1×3	7140	121.4	80.7	94.7	82.2	95.5
MViT-B, 32×3 [13]	-	32×3	1×5	850	36.6	80.2	94.4	83.8	96.3
MViT-B, 64×3 [13]	-	64×3	3×3	4095	36.6	81.2	95.1	-	-
VidTr-L [63]	ImageNet-21K	32×2	10×3	10530	-	78.6	93.5	-	-
X-ViT ($16 \times$) [4]	ImageNet-21K	16×4	1×3	850	-	80.2	94.7	84.5	96.3
ViViT-L/ 16×2 [1]	ImageNet-21K	32×2	4×3	17352	310.8	80.6	94.7	82.5	95.6
ViViT-L/ 16×2 [1]	JFT-300M	32×2	4×3	17352	310.8	82.8	95.5	84.3	96.2
Swin-T [38]	ImageNet-1K	32×2	4×3	1056	28.2	78.8	93.6	-	-
Swin-S [38]	ImageNet-1K	32×2	4×3	1992	49.8	80.6	94.5	-	-
Swin-B [38]	ImageNet-1K	32×2	4×3	3384	88.1	80.6	94.6	-	-
Swin-B [38]	ImageNet-21K	32×2	4×3	3384	88.1	82.7	95.5	84.0	96.5
DualFormer-T (ours)	ImageNet-1K	32×2	4×1	240	21.8	79.5	94.1	-	-
DualFormer-S (ours)	ImageNet-1K	32×2	4×1	636	48.9	80.6	94.9	-	-
DualFormer-B (ours)	ImageNet-1K	32×2	4×1	1072	86.8	81.1	95.0	-	-
DualFormer-B (ours)	ImageNet-21K	32×2	4×1	1072	86.8	82.9	95.5	85.2	96.6

Table 1. Comparisons with state-of-the-art methods for action recognition on Kinetics-400/600. All models are trained and evaluated on 224×224 spatial resolution. $n \times s$ input indicates we feed n frames to the network sampled every s frames. FLOPs indicates the total floating point operations per second during inference. The magnitudes are Giga (10^9) and Mega (10^6) for FLOPs and Param, respectively.

4. Experiments

4.1. Datasets

We evaluate our approach on five popular video datasets. For action recognition, we utilize two versions of Kinetics [28]. **Kinetics-400** and **Kinetics-600** contain approximately 240K/370K training videos and 20k/28k validation videos. These videos are labeled using 400 and 600 action classes, respectively. For temporal modeling, as the widely-used dataset Something-Something [16] has expired, we conduct experiments on another fine-grained action benchmark called **Diving-48** [32], which consists of ~ 18 k videos with 48 diving classes. Finally, we examine transfer learning performance of our method on two smaller datasets, including **HMDB-51** [31] and **UCF-101** [46].

4.2. Implementation Details

Unless otherwise stated, our model receives a clip of 32 frames sampled from the original video using a temporal stride of 2 and spatial resolution of 224×224 , leading to $16 \times 56 \times 56$ visual tokens at the first stage. During inference, four temporal clips with a center crop (i.e., a total of four space-time views) are exploited to compute accuracy.

Kinetics-400/600. For both Kinetics datasets, DualFormer is trained for 30 epochs with a batch size 64, using an AdamW [29] optimizer and a cosine learning rate scheduler. Following Swin [38], we utilize different initial learning rates for the ImageNet-pretrained backbone ($1e-4$) and head ($1e-3$). The first 2.5 epochs are used for a linear warm-

up. To avoid overfitting, we set weight decay to 0.02, 0.02, 0.05 and stochastic depth drop rates [22] to 0.1, 0.2 and 0.3 for the tiny, small and base versions, respectively. Token labelling [26] is employed as augmentation to improve DualFormer-T/S. See more details in Appendix A.3.

Diving/HMDB/UCF. For the other datasets, we employ an AdamW [29] optimizer for shorter training of 16 epochs with one epoch of linear warm-up. The learning rate, batch size, weight decay and stochastic depth drop rate are the same as those of Kinetics. We use the pretrained weights on ImageNet-1K or Kinetics-400 for the model initialization.

4.3. Comparison to State-of-the-art

Kinetics-400. We present the top-1 and top-5 accuracy of CNNs (upper part) and transformer-based methods (lower part) in Table 1. Compared to the best CNN-based method X3D-XXL [58], DualFormer-S achieves slightly higher accuracy while using $9.2 \times$ fewer FLOPs. Compared to transformers (MViT-B, 32×3 [13] and X-ViT [4]), DualFormer-S with similar computations brings $\sim 0.4\%$ gain on the top-1 accuracy. In contrast to Swin-T [38], DualFormer-T outperforms it by 0.7% on top-1 and 0.5% on top-5 score with $4.4 \times$ fewer computational costs. We also witness 1.8% improvement on the top-1 accuracy when using ImageNet-21K to pretrain DualFormer-B compared to ImageNet-1K. With ImageNet-21K pretraining, DualFormer-B achieves the state-of-the-art results on both metrics while being dramatically faster than two recent transformer backbones: $16.2 \times$ faster than ViViT-L [1] and $3.2 \times$ faster than Swin-

B [38]. See more details on accuracy vs. speed in Fig. 1. **Kinetics-600.** As shown in Table 1, the results on Kinetics-600 are similar to those on the former dataset. DualFormer-B achieves the highest accuracy among these models. In particular, DualFormer-B brings **1.2%** gains on top-1 score and runs $3.2\times$ faster than Swin-B. Compared to ViViT-L which is pretrained on a large-scale and private dataset JFM-300M, although our DualFormer-B is pretrained on a much smaller dataset (ImageNet-21K), it yields **0.9%** higher top-1 accuracy and requires **16.2** \times fewer FLOPs.

Diving-48. Then, we train our model on a temporally-heavy dataset. Due to a recently reported label issue of Diving-48, we only compare our model with SlowFast [15] and TimeSformer [3]. From Table 2, we observe that our DualFormer obtains a maximum **81.8%** top-1 score on Diving-48, considerably surpassing SlowFast. Even compared to TimeSformer-L which possesses **3.7** \times FLOPs and receives 96 frames as input, our method yields **0.8%** higher accuracy while using only 32 frames as input. These results verify the strong power of our model in temporal modeling.

HMDB-51 and UCF-101. Lastly, we examine the transfer learning ability of our DualFormer over the split 1 of HMDB-51 and UCF-101. The top-1 accuracy of each method is reported in Table 2. By using ImageNet-1K pretrained weights for initialization, the tiny version achieves comparable performance to VidTr-M [63] while using **192** \times fewer FLOPs (see DualFormer-T* in Table 2). When pretrained on Kinetics-400, DualFormer-S with 12 testing views can outperform VidTr-L by a large margin on both datasets (**2%** and **0.8%** higher score on HMDB and UCF) using only **18%** of the FLOPs, revealing the generalization potential of our model on small datasets.

Method	Input	Views	FLOPs	DIV	HMDB	UCF
I3D [6]	64 \times 1	-	-	-	74.3	95.1
TSM [34]	8	-	-	-	70.7	94.5
TeiNet [37]	16	-	-	-	73.3	96.7
SlowFast [15]	16 \times 8	-	-	77.6	-	-
VidTr-M [63]	16 \times 4	10 \times 3	5370	-	74.4	96.6
VidTr-L [63]	32 \times 4	10 \times 3	10530	-	74.4	96.7
TimeSformer [3]	8 \times 4	1 \times 3	590	75.0	-	-
TimeSformer-L [3]	96 \times 4	1 \times 3	7140	81.0	-	-
DualFormer-T*	16 \times 4	4 \times 1	28	75.4	74.6	96.3
DualFormer-T	16 \times 4	4 \times 1	28	75.9	75.0	96.6
DualFormer-S	32 \times 4	4 \times 1	636	81.2	76.2	97.4
DualFormer-S	32 \times 4	4 \times 3	1908	81.8	76.4	97.5

Table 2. Results on HMDB-51, UCF-101 and Diving-48 (DIV). Baseline results are from [3, 63]. We pretrain our models on Kinetics-400 and finetune them on these datasets, only except for DualFormer-T* which is pretrained on ImageNet-1K.

4.4. Ablation Study

Effect of LW-MSA & GP-MSA. To study the effect of the proposed dual-level MSA, we test different combinations of LW-MSA and GP-MSA based on DualFormer-T. As shown

in Figure 3, (LG, LG, LG, LG) denotes our default configuration where each block sequentially performs LW-MSA and GP-MSA. For the four variants at the upper part of Table 3, LL and GG mean that the blocks at that stage only contain two LW-MSAs and two GP-MSAs, respectively. For example, (LL, LL, LG, LG) means using blocks with two LW-MSAs at the first two stages and using a combination of LW-MSA and GP-MSA at the last two stages.

For a fair comparison, we slightly tune the hyperparameter to ensure their FLOPs and parameters to be similar. We report the accuracy of these variants on Kinetics-400 in the upper part of Table 3. Among these variants, (GG, GG, GG, GG) performs the worst since the local context information is very important to a patch. The model with only LW-MSA degrades by 1.1% top-1 score (79.5% \rightarrow 78.4%) due to a limited receptive field at every stage. By integrating GP-MSA to increase the receptive field, both (LL, LL, LG, LG) and (LG, LG, LL, LL) achieve better performance than the variants with only local or global modules. In particular, adding GP-MSA to the early stages benefits more than late stages, revealing the importance of GP-MSA to complement the early stages. Moreover, we evaluate the two pyramid scales in GP-MSA and report their results in the lower part of Table 3. Compared to our default setting, we can find a clear accuracy drop by removing either the (4, 4, 4) or (8, 7, 7) scale. Besides, some examples of attention visualization are shown in Figure 6.

Variants	FLOPs	Param	Top-1	Top-5
(LL, LL, LL, LL)	244	21.7	78.4	93.3
(GG, GG, GG, GG)	228	21.8	77.6	93.2
(LL, LL, LG, LG)	236	21.7	78.8	93.5
(LG, LG, LL, LL)	244	21.8	79.3	94.0
(LG ₁ , LG ₁ , LG ₁ , LG ₁)	224	21.8	78.4	93.4
(LG ₂ , LG ₂ , LG ₂ , LG ₂)	232	21.8	79.3	93.9
(LG, LG, LG, LG)	240	21.8	79.5	94.1

Table 3. Results of different combinations of LW-MSA (L) and GP-MSA (G) with DualFormer-T on Kinetics-400. G₁ and G₂ denote GP-MSA with only one pyramid scale (4,4,4) and (8,7,7), respectively. The gray row indicates our default setting.

Effect of testing views. Previous methods employ multiple space-time views to boost performance during inference, e.g., 10 \times 3 views in VidTr-L and 4 \times 3 views in Swin. We investigate how the number of testing views affects the accuracy of DualFormer-T on Kinetics-400 and Diving-48. From Figure 5, we notice that increasing the number of temporal clips can bring significant improvement on both datasets. Besides, using more spatial crops does not always help. For example, using three spatial crops slightly outperforms the 1-crop counterpart on Diving-48. As the inference FLOPs is proportional to the space-time views, to trade off the computational costs and accuracy, our method uses a testing strategy of four temporal clips with a spatial crop (totally four space-time views) during the inference phase.

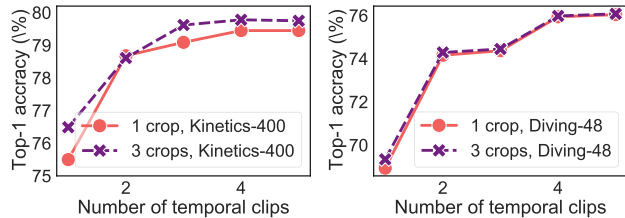


Figure 5. Effect of temporal clips and spatial crops during inference. Left: Results on Kinetics-400. Right: Results on Diving-48.

Effect of window size in LW-MSA. Window size is a crucial hyperparameter in LW-MSA. Hence, we test different window sizes to investigate their effect on model performance. As shown in Table 4, a larger window size in both temporal and spatial dimensions brings consistent gains in accuracy due to the increase of local receptive field, but also induces heavier computation. For an accuracy-speed balance, we choose $(8, 7, 7)$ as our default setting. From this table, we also observe that reducing the number of input frames (e.g., $32 \rightarrow 16$) can dramatically improve efficiency but inevitably degrades the top-1 accuracy by $\sim 1\%$.

Input	Window Size	FLOPs	Top-1	Top-5
16×4	$4 \times 7 \times 7$	104	78.0	93.2
16×4	$8 \times 7 \times 7$	112	78.4	93.3
32×2	$4 \times 7 \times 7$	224	79.1	93.9
32×2	$8 \times 7 \times 7$	240	79.5	94.1
32×2	$16 \times 7 \times 7$	272	79.7	94.4
32×2	$8 \times 14 \times 14$	324	79.7	94.5

Table 4. Effect of window size of LW-MSA with DualFormer-T on Kinetic-400. The gray row indicates the default configuration.

Effect of pyramid downsampling function. There are several alternative functions to generate global priors in GP-MSA, such as average pooling (AvgPool) and standard convolution (Conv). Here, we replace the depth-wise convolution (DWConv) with them on Kinetics-400 to see their effect. As depicted in Table 5, our DWConv achieves comparable performance to Conv while using much fewer parameters. Our implementation also outperforms AvgPool by 0.8% on the top-1 score with similar computation costs.

Do we need PEG? Next, we study the effect of the PEG module which allows position-aware MSA. As illustrated in Table 6, DualFormer without PEG suffers from a clear drop on top-1 accuracy ($79.5\% \rightarrow 78.9\%$), which indicates the necessity of integrating position information in MSA. We fur-

Method	FLOPs	Param	Top-1
AvgPool	59	21.8	78.7
Conv	61	27.6	79.5
DWConv	60	21.8	79.5

Table 5. Results of different pyramid downsampling functions based on DualFormer-T on Kinetics-400.

Method	Top-1
w.o PEG	78.9
Swin [38]	79.3
DWConv	79.5

Table 6. Effect of PEGs to DualFormer-T on Kinetics-400..

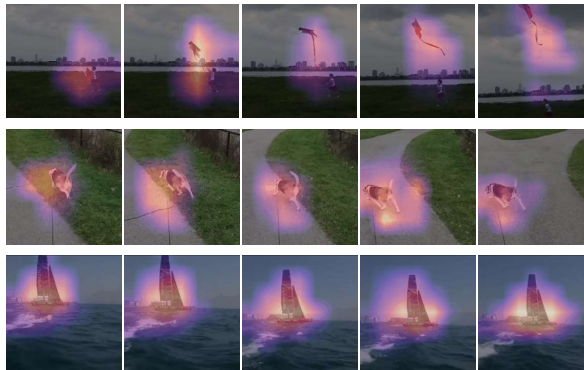


Figure 6. Visualization of attention maps at the last layer generated by Grad-CAM [44] on Kinetics-400. Our model successfully learns to focus on the relevant parts in the video clip. Upper: flying kites. Middle: walking dogs. Below: sailing.

ther compare our DWConv-based PEG with a relative bias-based method in the state-of-the-art method (Swin). As shown in Figure 6, our solution achieves 0.2% higher top-1 score than the relative position embedding in Swin.

Effect of Temporal Pooling Rate. Following the previous attempts [13, 38], our architecture utilizes a multi-scale hierarchy in different stages to produce decreasing-resolution feature maps from early to late stages. Such hierarchy is achieved by the patch merging layer at the beginning of the last three stages, where we downsample the spatial size of feature map by $2 \times$ and keep the original temporal resolution. Here, we discuss the effect of temporal pooling at the last three stages. According to the results in Table 7, even though such temporal pooling can further reduce the computational cost, it leads to a decrease in the overall accuracy.

Pooling Rate	Patch Size	FLOPs	Param	Top-1	Top-5
1, 1, 1	(4, 4, 4)	112	21.8	78.5	93.3
2, 1, 1	(2, 4, 4)	136	21.8	78.7	93.5
1, 2, 1	(2, 4, 4)	152	21.9	78.8	93.5
1, 1, 2	(2, 4, 4)	216	22.3	79.2	93.9
1, 1, 1	(2, 4, 4)	240	21.8	79.5	94.1

Table 7. Effect of temporal pooling in DualFormer-T on Kinetic-400. The pooling rate (i, j, k) denotes decreasing the temporal resolution i, j and k times at the last three stages, respectively.

5. Conclusion

In this paper, we develop a transformer-based architecture with local-global attention stratification for efficient video recognition. Empirical study demonstrates that the proposed method achieves a better accuracy-speed trade-off on five popular video recognition datasets. We will release the code for public use soon. In the future, we plan to remove the strong dependency on pretrained models and design a useful strategy to train our model from scratch. Another direction is to explore the use of our model in other applications, such as video segmentation and prediction.

Acknowledgement

The authors would like to thank Quanhong Fu at Sea AI Lab for the help to improve the technical writing aspect of this paper. This research is supported by Singapore Ministry of Education Academic Research Fund Tier 2 under MOE’s official grant number MOE2018-T2-1-103.

References

- [1] Anurag Arnab, Mostafa Dehghani, Georg Heigold, Chen Sun, Mario Lučić, and Cordelia Schmid. Vivit: A video vision transformer. *arXiv preprint arXiv:2103.15691*, 2021. [1](#), [2](#), [3](#), [5](#), [6](#), [12](#), [13](#)
- [2] Jimmy Lei Ba, Jamie Ryan Kiros, and Geoffrey E Hinton. Layer normalization. *arXiv preprint arXiv:1607.06450*, 2016. [4](#)
- [3] Gedas Bertasius, Heng Wang, and Lorenzo Torresani. Is space-time attention all you need for video understanding? *arXiv preprint arXiv:2102.05095*, 2021. [1](#), [2](#), [3](#), [5](#), [6](#), [7](#), [12](#), [13](#)
- [4] Adrian Bulat, Juan-Manuel Perez-Rua, Swathikiran Sudhakaran, Brais Martinez, and Georgios Tzimiropoulos. Space-time mixing attention for video transformer. *arXiv preprint arXiv:2106.05968*, 2021. [3](#), [5](#), [6](#), [12](#), [13](#)
- [5] Joao Carreira and Andrew Zisserman. Quo vadis, action recognition? a new model and the kinetics dataset. In *proceedings of the IEEE Conference on Computer Vision and Pattern Recognition*, pages 6299–6308, 2017. [1](#)
- [6] Joao Carreira and Andrew Zisserman. Quo vadis, action recognition? a new model and the kinetics dataset. In *proceedings of the IEEE Conference on Computer Vision and Pattern Recognition*, pages 6299–6308, 2017. [1](#), [3](#), [6](#), [7](#), [12](#)
- [7] Chun-Fu Chen, Rameswar Panda, and Quanfu Fan. Regionvit: Regional-to-local attention for vision transformers. *arXiv preprint arXiv:2106.02689*, 2021. [2](#), [5](#), [12](#)
- [8] François Chollet. Xception: Deep learning with depthwise separable convolutions. In *Proceedings of the IEEE conference on computer vision and pattern recognition*, pages 1251–1258, 2017. [5](#)
- [9] Xiangxiang Chu, Zhi Tian, Yuqing Wang, Bo Zhang, Haibing Ren, Xiaolin Wei, Huaxia Xia, and Chunhua Shen. Twins: Revisiting the design of spatial attention in vision transformers. In *NeurIPS 2021*, 2021. [2](#), [3](#), [5](#), [12](#)
- [10] Xiangxiang Chu, Zhi Tian, Bo Zhang, Xinlong Wang, Xiaolin Wei, Huaxia Xia, and Chunhua Shen. Conditional positional encodings for vision transformers. *arXiv preprint arXiv:2102.10882*, 2021. [5](#)
- [11] Jia Deng, Wei Dong, Richard Socher, Li-Jia Li, Kai Li, and Li Fei-Fei. Imagenet: A large-scale hierarchical image database. In *2009 IEEE conference on computer vision and pattern recognition*, pages 248–255. Ieee, 2009. [12](#)
- [12] Alexey Dosovitskiy, Lucas Beyer, Alexander Kolesnikov, Dirk Weissenborn, Xiaohua Zhai, Thomas Unterthiner, Mostafa Dehghani, Matthias Minderer, Georg Heigold, Sylvain Gelly, et al. An image is worth 16x16 words: Transformers for image recognition at scale. In *International Conference on Learning Representations*, 2020. [1](#), [3](#), [12](#)
- [13] Haoqi Fan, Bo Xiong, Karttikeya Mangalam, Yanghao Li, Zhicheng Yan, Jitendra Malik, and Christoph Feichtenhofer. Multiscale vision transformers. *arXiv preprint arXiv:2104.11227*, 2021. [1](#), [3](#), [5](#), [6](#), [8](#)
- [14] Christoph Feichtenhofer. X3d: Expanding architectures for efficient video recognition. In *Proceedings of the IEEE/CVF Conference on Computer Vision and Pattern Recognition*, pages 203–213, 2020. [1](#), [3](#), [6](#)
- [15] Christoph Feichtenhofer, Haoqi Fan, Jitendra Malik, and Kaiming He. Slowfast networks for video recognition. In *Proceedings of the IEEE/CVF international conference on computer vision*, pages 6202–6211, 2019. [1](#), [3](#), [6](#), [7](#)
- [16] Raghav Goyal, Samira Ebrahimi Kahou, Vincent Michalski, Joanna Materzynska, Susanne Westphal, Heuna Kim, Valentin Haenel, Ingo Fruend, Peter Yianilos, Moritz Mueller-Freitag, et al. The” something something” video database for learning and evaluating visual common sense. In *Proceedings of the IEEE international conference on computer vision*, pages 5842–5850, 2017. [6](#)
- [17] Kensho Hara, Hirokatsu Kataoka, and Yutaka Satoh. Learning spatio-temporal features with 3d residual networks for action recognition. In *Proceedings of the IEEE International Conference on Computer Vision Workshops*, pages 3154–3160, 2017. [3](#)
- [18] Kensho Hara, Hirokatsu Kataoka, and Yutaka Satoh. Can spatiotemporal 3d cnns retrace the history of 2d cnns and imagenet? In *Proceedings of the IEEE conference on Computer Vision and Pattern Recognition*, pages 6546–6555, 2018. [3](#)
- [19] Kaiming He, Xiangyu Zhang, Shaoqing Ren, and Jian Sun. Spatial pyramid pooling in deep convolutional networks for visual recognition. *IEEE transactions on pattern analysis and machine intelligence*, 37(9):1904–1916, 2015. [4](#)
- [20] Kaiming He, Xiangyu Zhang, Shaoqing Ren, and Jian Sun. Deep residual learning for image recognition. In *Proceedings of the IEEE conference on computer vision and pattern recognition*, pages 770–778, 2016. [1](#), [3](#)
- [21] Somboon Hongeng, Ram Nevatia, and Francois Bremond. Video-based event recognition: activity representation and probabilistic recognition methods. *Computer Vision and Image Understanding*, 96(2):129–162, 2004. [1](#)
- [22] Gao Huang, Yu Sun, Zhuang Liu, Daniel Sedra, and Kilian Q Weinberger. Deep networks with stochastic depth. In *European conference on computer vision*, pages 646–661. Springer, 2016. [6](#)
- [23] Shuiwang Ji, Wei Xu, Ming Yang, and Kai Yu. 3d convolutional neural networks for human action recognition. *IEEE transactions on pattern analysis and machine intelligence*, 35(1):221–231, 2012. [3](#)
- [24] Boyuan Jiang, MengMeng Wang, Weihao Gan, Wei Wu, and Junjie Yan. Stm: Spatiotemporal and motion encoding for action recognition. In *Proceedings of the IEEE/CVF International Conference on Computer Vision*, pages 2000–2009, 2019. [3](#)
- [25] Zihang Jiang, Qibin Hou, Li Yuan, Zhou Daquan, Yujun Shi, Xiaojie Jin, Anran Wang, and Jiashi Feng. All tokens matter: Token labeling for training better vision transformers. In *Thirty-Fifth Conference on Neural Information Processing Systems*, 2021. [12](#), [13](#)

- [26] Zihang Jiang, Qibin Hou, Li Yuan, Daquan Zhou, Xiaojie Jin, Anran Wang, and Jiashi Feng. Token labeling: Training a 85.5% top-1 accuracy vision transformer with 56m parameters on imagenet. *arXiv preprint arXiv:2104.10858*, 2021. **6**
- [27] Andrej Karpathy, George Toderici, Sanketh Shetty, Thomas Leung, Rahul Sukthankar, and Li Fei-Fei. Large-scale video classification with convolutional neural networks. In *Proceedings of the IEEE conference on Computer Vision and Pattern Recognition*, pages 1725–1732, 2014. **3**
- [28] Will Kay, Joao Carreira, Karen Simonyan, Brian Zhang, Chloe Hillier, Sudheendra Vijayanarasimhan, Fabio Viola, Tim Green, Trevor Back, Paul Natsev, et al. The kinetics human action video dataset. *arXiv preprint arXiv:1705.06950*, 2017. **2, 3, 6, 12**
- [29] Diederik P Kingma and Jimmy Ba. Adam: A method for stochastic optimization. *arXiv preprint arXiv:1412.6980*, 2014. **6, 12**
- [30] Alex Krizhevsky, Ilya Sutskever, and Geoffrey E Hinton. Imagenet classification with deep convolutional neural networks. *Advances in neural information processing systems*, 25:1097–1105, 2012. **1, 2, 3, 12**
- [31] Hildegard Kuehne, Hueihan Jhuang, Estíbaliz Garrote, Tomaso Poggio, and Thomas Serre. Hmdb: a large video database for human motion recognition. In *2011 International conference on computer vision*, pages 2556–2563. IEEE, 2011. **6**
- [32] Yingwei Li, Yi Li, and Nuno Vasconcelos. Resound: Towards action recognition without representation bias. In *Proceedings of the European Conference on Computer Vision (ECCV)*, pages 513–528, 2018. **6**
- [33] Zewen Li, Fan Liu, Wenjie Yang, Shouheng Peng, and Jun Zhou. A survey of convolutional neural networks: analysis, applications, and prospects. *IEEE Transactions on Neural Networks and Learning Systems*, 2021. **2**
- [34] Ji Lin, Chuang Gan, and Song Han. Tsm: Temporal shift module for efficient video understanding. In *Proceedings of the IEEE/CVF International Conference on Computer Vision*, pages 7083–7093, 2019. **1, 3, 7**
- [35] Min Lin, Qiang Chen, and Shuicheng Yan. Network in network. In Yoshua Bengio and Yann LeCun, editors, *2nd International Conference on Learning Representations, ICLR 2014, Banff, AB, Canada, April 14-16, 2014, Conference Track Proceedings*, 2014. **4**
- [36] Ze Liu, Yutong Lin, Yue Cao, Han Hu, Yixuan Wei, Zheng Zhang, Stephen Lin, and Baining Guo. Swin transformer: Hierarchical vision transformer using shifted windows. *International Conference on Computer Vision (ICCV)*, 2021. **1, 2, 3, 12**
- [37] Zhaoyang Liu, Donghao Luo, Yabiao Wang, Limin Wang, Ying Tai, Chengjie Wang, Jilin Li, Feiyue Huang, and Tong Lu. Teinet: Towards an efficient architecture for video recognition. In *Proceedings of the AAAI Conference on Artificial Intelligence*, volume 34, pages 11669–11676, 2020. **3, 7**
- [38] Ze Liu, Jia Ning, Yue Cao, Yixuan Wei, Zheng Zhang, Stephen Lin, and Han Hu. Video swin transformer. *arXiv preprint arXiv:2106.13230*, 2021. **1, 2, 3, 4, 5, 6, 7, 8, 12, 13**
- [39] Zhaoyang Liu, Limin Wang, Wayne Wu, Chen Qian, and Tong Lu. Tam: Temporal adaptive module for video recognition. In *Proceedings of the IEEE/CVF International Conference on Computer Vision*, pages 13708–13718, 2021. **3**
- [40] Daniel Neimark, Omri Bar, Maya Zohar, and Dotan Asselmann. Video transformer network. *arXiv preprint arXiv:2102.00719*, 2021. **1, 3, 6**
- [41] Mandela Patrick, Dylan Campbell, Yuki M Asano, Ishan Misra Florian Metze, Christoph Feichtenhofer, Andrea Vedaldi, Jo Henriques, et al. Keeping your eye on the ball: Trajectory attention in video transformers. *arXiv preprint arXiv:2106.05392*, 2021. **3**
- [42] Zhaofan Qiu, Ting Yao, and Tao Mei. Learning spatio-temporal representation with pseudo-3d residual networks. In *proceedings of the IEEE International Conference on Computer Vision*, pages 5533–5541, 2017. **3**
- [43] René Ranftl, Alexey Bochkovskiy, and Vladlen Koltun. Vision transformers for dense prediction. In *Proceedings of the IEEE/CVF International Conference on Computer Vision*, pages 12179–12188, 2021. **1**
- [44] Ramprasaath R Selvaraju, Michael Cogswell, Abhishek Das, Ramakrishna Vedantam, Devi Parikh, and Dhruv Batra. Grad-cam: Visual explanations from deep networks via gradient-based localization. In *Proceedings of the IEEE international conference on computer vision*, pages 618–626, 2017. **8**
- [45] Karen Simonyan and Andrew Zisserman. Very deep convolutional networks for large-scale image recognition. *arXiv preprint arXiv:1409.1556*, 2014. **1, 3**
- [46] Khurram Soomro, Amir Roshan Zamir, and Mubarak Shah. Ucf101: A dataset of 101 human actions classes from videos in the wild. *arXiv preprint arXiv:1212.0402*, 2012. **6**
- [47] Waldo R Tobler. A computer movie simulating urban growth in the detroit region. *Economic geography*, 46(sup1):234–240, 1970. **1**
- [48] Hugo Touvron, Matthieu Cord, Matthijs Douze, Francisco Massa, Alexandre Sablayrolles, and Hervé Jégou. Training data-efficient image transformers & distillation through attention. In *International Conference on Machine Learning*, pages 10347–10357. PMLR, 2021. **3, 12**
- [49] Du Tran, Lubomir Bourdev, Rob Fergus, Lorenzo Torresani, and Manohar Paluri. Learning spatiotemporal features with 3d convolutional networks. In *Proceedings of the IEEE international conference on computer vision*, pages 4489–4497, 2015. **1, 3**
- [50] Du Tran, Heng Wang, Lorenzo Torresani, and Matt Feiszli. Video classification with channel-separated convolutional networks. In *Proceedings of the IEEE/CVF International Conference on Computer Vision*, pages 5552–5561, 2019. **3, 6**
- [51] Du Tran, Heng Wang, Lorenzo Torresani, Jamie Ray, Yann LeCun, and Manohar Paluri. A closer look at spatiotemporal convolutions for action recognition. In *Proceedings of the IEEE conference on Computer Vision and Pattern Recognition*, pages 6450–6459, 2018. **1, 3, 5, 6**
- [52] Ashish Vaswani, Noam Shazeer, Niki Parmar, Jakob Uszkoreit, Llion Jones, Aidan N Gomez, Łukasz Kaiser, and Illia

- Polosukhin. Attention is all you need. In *Advances in neural information processing systems*, pages 5998–6008, 2017. [1](#), [5](#)
- [53] Huiyu Wang, Yukun Zhu, Hartwig Adam, Alan Yuille, and Liang-Chieh Chen. Max-deeplab: End-to-end panoptic segmentation with mask transformers. In *Proceedings of the IEEE/CVF Conference on Computer Vision and Pattern Recognition*, pages 5463–5474, 2021. [1](#)
- [54] Limin Wang, Yuanjun Xiong, Zhe Wang, Yu Qiao, Dahua Lin, Xiaoou Tang, and Luc Van Gool. Temporal segment networks for action recognition in videos. *IEEE transactions on pattern analysis and machine intelligence*, 41(11):2740–2755, 2018. [3](#)
- [55] Wenhai Wang, Enze Xie, Xiang Li, Deng-Ping Fan, Kaitao Song, Ding Liang, Tong Lu, Ping Luo, and Ling Shao. Pyramid vision transformer: A versatile backbone for dense prediction without convolutions. *arXiv preprint arXiv:2102.12122*, 2021. [1](#), [12](#)
- [56] Xiaolong Wang, Ross Girshick, Abhinav Gupta, and Kaiming He. Non-local neural networks. In *Proceedings of the IEEE conference on computer vision and pattern recognition*, pages 7794–7803, 2018. [5](#)
- [57] Yuqing Wang, Zhaoliang Xu, Xinlong Wang, Chunhua Shen, Baoshan Cheng, Hao Shen, and Huaxia Xia. End-to-end video instance segmentation with transformers. In *Proceedings of the IEEE/CVF Conference on Computer Vision and Pattern Recognition*, pages 8741–8750, 2021. [1](#)
- [58] Saining Xie, Chen Sun, Jonathan Huang, Zhuowen Tu, and Kevin Murphy. Rethinking spatiotemporal feature learning: Speed-accuracy trade-offs in video classification. In *Proceedings of the European conference on computer vision (ECCV)*, pages 305–321, 2018. [3](#), [6](#)
- [59] Huijuan Xu, Abir Das, and Kate Saenko. R-c3d: Region convolutional 3d network for temporal activity detection. In *Proceedings of the IEEE international conference on computer vision*, pages 5783–5792, 2017. [3](#)
- [60] Jianwei Yang, Chunyuan Li, Pengchuan Zhang, Xiyang Dai, Bin Xiao, Lu Yuan, and Jianfeng Gao. Focal self-attention for local-global interactions in vision transformers. *arXiv preprint arXiv:2107.00641*, 2021. [2](#), [3](#)
- [61] Li Yuan, Qibin Hou, Zihang Jiang, Jiashi Feng, and Shuicheng Yan. Volo: Vision outlooker for visual recognition. *arXiv preprint arXiv:2106.13112*, 2021. [13](#)
- [62] Xuefan Zha, Wentao Zhu, Tingxun Lv, Sen Yang, and Ji Liu. Shifted chunk transformer for spatio-temporal representational learning. *arXiv preprint arXiv:2108.11575*, 2021. [3](#)
- [63] Yanyi Zhang, Xinyu Li, Chunhui Liu, Bing Shuai, Yi Zhu, Biagio Brattoli, Hao Chen, Ivan Marsic, and Joseph Tighe. Vidtr: Video transformer without convolutions. In *Proceedings of the IEEE/CVF International Conference on Computer Vision*, pages 13577–13587, 2021. [3](#), [6](#), [7](#)
- [64] Xizhou Zhu, Weijie Su, Lewei Lu, Bin Li, Xiaogang Wang, and Jifeng Dai. Deformable detr: Deformable transformers for end-to-end object detection. *arXiv preprint arXiv:2010.04159*, 2020. [1](#)

A. Additional Implementation Details

To support the reproducibility of the results in this study, we will release our code at <https://github.com/sail-sg/dualformer>. In the main body of our paper, we have illustrated the implementation details on the five video datasets. Here, we will introduce the pretraining settings in Sec. A.1 and A.2 and more implementation details of our model in Sec. A.3 and A.4.

A.1. Initialization by Pretrained Models

Vision Transformer (ViT) [12, 48] and its variants [7, 9, 36, 55] have achieved promising results on image classification when trained on large-scale datasets, since transformers lack some of the inductive biases of CNNs. Nevertheless, even the largest video dataset such as Kinetics [28] have much fewer labelled instances than these image counterparts, e.g., ImageNet [11, 30], making it extremely challenging to train a video transformer from scratch [1, 4].

To tackle this challenge, we follow existing video transformers [1, 3, 4, 38] to utilize a pretrained 2D model (e.g., pretrained on ImageNet) as the initialization of our 3D model. Then, we can fine-tune it on the video datasets for the recognition tasks. In contrast to the pretrained 2D DualFormer, only three building blocks in 3D DualFormer are in different shapes – 1) the patch embedding layer at the first stage; 2) the depth-wise convolution for generating position embeddings in PEG at each stage; and 3) the depth-wise convolution for constructing global priors in GP-MSA. Note that all these three blocks are composed of convolution operations, we thereby employ the common approach [6] for initializing 3D convolution kernels from 2D filters, i.e., we *inflate* the 2D convolution kernels by replicating the filters along the temporal dimension and averaging them.

A.2. Pretraining Settings on ImageNet

When pretraining our DualFormer on ImageNet-1K, we mostly follow the settings of DeiT [48] and Swin [36]. To be more specific, we employ an AdamW optimizer [29] for 300 epochs together with a cosine decay learning rate scheduler and 20 epochs of linear warm-up. The batch size is set to 1024, and the initial learning rate is 0.001. To avoid overfitting, a weight decay rate of 0.05 is used in our method. We include most of the augmentation and regularization strategies of [48] in training, except for repeated augmentation and exponential moving average (EMA), which has been verified ineffective in Swin [36].

For DualFormer-B, we also pretrain it on the larger version of ImageNet, i.e., the ImageNet-21K dataset which contains 14.2 million images and 22 thousand classes. Following Swin Transformer [36], we utilize an AdamW optimizer for 100 epochs using a linear decay learning rate scheduler with a 5-epoch linear warm-up strategy. A batch

size of 1024, an initial learning rate of $5e-4$, and a weight decay of 0.01 are used. We also employ a stochastic depth drop rate 0.2 to improve its generalization ability.

A.3. Additional Training Details

We implement our models via PyTorch 1.9.0 and mmaction2 which is an open-source toolbox for video understanding. All models are trained on 8 Nvidia A100 GPUs. For example, training a DualFormer-T on Kinetics-400 takes ~ 31 hours on 8 A100 GPUs, while training a larger model DualFormer-B on Kinetics-400 requires ~ 3 days on 8 A100 GPUs. For the small models (i.e., DualFormer-T/S) on Kinetics-400, we utilize a variant² of token labelling [25] as an additional augmentation method to improve their performance, using our DualFormer-B as the annotation model (see Sec B.1 for its effects).

A.4. Configuration Details

In Table 8, we provide the configuration details of each version of the proposed model.

Stage	Layer	Tiny	Small	Base
Stage 1	Patch Merging	$p_1 = (2, 4, 4)$ $C_1 = 64$	$p_1 = (2, 4, 4)$ $C_1 = 96$	$p_1 = (2, 4, 4)$ $C_1 = 128$
	Output: $\frac{T}{2}, \frac{H}{4}, \frac{W}{4}$	LW-MSA GP-MSA $\begin{bmatrix} (8, 7, 7) \\ (4, 4, 4) \\ (8, 7, 7) \end{bmatrix} \times 1$	$\begin{bmatrix} (8, 7, 7) \\ (4, 4, 4) \\ (8, 7, 7) \end{bmatrix} \times 1$	$\begin{bmatrix} (8, 7, 7) \\ (4, 4, 4) \\ (8, 7, 7) \end{bmatrix} \times 1$
Stage 2	Patch Merging	$p_2 = (1, 2, 2)$ $C_2 = 128$	$p_2 = (1, 2, 2)$ $C_2 = 192$	$p_2 = (1, 2, 2)$ $C_2 = 256$
	Output: $\frac{T}{2}, \frac{H}{8}, \frac{W}{8}$	LW-MSA GP-MSA $\begin{bmatrix} (8, 7, 7) \\ (4, 4, 4) \\ (8, 7, 7) \end{bmatrix} \times 1$	$\begin{bmatrix} (8, 7, 7) \\ (4, 4, 4) \\ (8, 7, 7) \end{bmatrix} \times 1$	$\begin{bmatrix} (8, 7, 7) \\ (4, 4, 4) \\ (8, 7, 7) \end{bmatrix} \times 1$
Stage 3	Patch Merging	$p_3 = (1, 2, 2)$ $C_3 = 256$	$p_3 = (1, 2, 2)$ $C_3 = 384$	$p_3 = (1, 2, 2)$ $C_3 = 512$
	Output: $\frac{T}{2}, \frac{H}{16}, \frac{W}{16}$	LW-MSA GP-MSA $\begin{bmatrix} (8, 7, 7) \\ (8, 7, 7) \end{bmatrix} \times 5$	$\begin{bmatrix} (8, 7, 7) \\ (8, 7, 7) \end{bmatrix} \times 9$	$\begin{bmatrix} (8, 7, 7) \\ (8, 7, 7) \end{bmatrix} \times 9$
Stage 4	Patch Merging	$p_4 = (1, 2, 2)$ $C_4 = 512$	$p_4 = (1, 2, 2)$ $C_4 = 768$	$p_4 = (1, 2, 2)$ $C_4 = 1024$
	Output: $\frac{T}{2}, \frac{H}{32}, \frac{W}{32}$	LW-MSA GP-MSA $\begin{bmatrix} (8, 7, 7) \\ (whole) \end{bmatrix} \times 2$	$\begin{bmatrix} (8, 7, 7) \\ (whole) \end{bmatrix} \times 1$	$\begin{bmatrix} (8, 7, 7) \\ (whole) \end{bmatrix} \times 1$

Table 8. Model configurations of DualFormer. p_i and C_i denote patch size and feature dimension at the i -th stage, respectively. “Whole” in the GP-MSA at stage 4 means to extract the global priors with the same shape as the input feature map due to the reduction of input video resolution.

B. More Experimental Results

B.1. Effects of Token labelling

In image processing, token labelling [25] assigns each patch token with an individual location-specific supervision generated by a machine annotator and reformulates the image classification problem into multiple token-level recognition problems. Here, we employ our based model

²MixToken [25] is turned off since it does not work in our experiments.

DualFormer-B as the annotator and explore the effects of token labelling on video recognition. As depicted in Table 9, DualFormer-T and DualFormer-S can achieve 0.5% and 0.3% higher top-1 score by using the token labelling trick, respectively. Although these improvements are not very significant compared to the image counterparts [25, 61], we believe designing a more powerful video-based token labelling would bring more considerable gains. We leave this for our future work.

Method	TokenLabel	Top-1 (%)	Top-5 (%)
DualFormer-T		79.0	93.7
DualFormer-T	✓	79.5	94.1
DualFormer-S		80.3	94.5
DualFormer-S	✓	80.6	94.9

Table 9. Effects of token labelling [25] on Kinetic-400.

C. Limitations

Even though we have verified the effectiveness of our proposed DualFormer through extensive experiments, our method still has space for improvement in terms of the following two aspects.

Limitation 1 (Pretrained model). Similar to the existing transformer-based architectures [1, 3, 4, 38], our DualFormer is heavily dependent on the pretrained dataset, i.e., ImageNet-1K/21K, resulting in a large additional training time. When training from scratch, all versions of our models suffer 20%~30% decrease in the top-1 accuracy on Kinetics-400. Hence, how to remove the strong dependency on pretrained models still remains an open problem.

Limitation 2 (FLOPs bottleneck). To improve efficiency, we have investigated the FLOPs of each layer in our DualFormer. We surprisingly find that the major bottleneck is the MLPs for non-linear transformation instead of the MSA computations, since we have greatly reduced the number of keys/values in MSA via our method. For example, DualFormer-T totally requires 60 GFLOPs during inference while ~50% of the FLOPs are from MLP computations. According to this observation, we have tried to reduce the MLP expansion rate from 4 to {1, 2, 3} and train the new models. However, the performance of DualFormer-T degrades by 5%~12% on the pretrained dataset. This fact verifies the importance of MLPs for non-linear transformation in a large feature space. Then, we also try to factorize the MLP weights into two lower-rank matrix for FLOPs reduction. Although such matrix factorization reduces 25% of the FLOPs, it causes ~1% drop in the top-1 score on Kinetics-400. Thus, it is still challenging to reduce the FLOPs of MLPs. We will continue to explore this direction.